ENHANCING IMAGE RESTORATION TRANSFORMER WITH ADAPTIVE TOKEN DICTIONARY

Anonymous authors
Paper under double-blind review

ABSTRACT

Image restoration is a classic computer vision problem that involves estimating high-quality (HQ) images from low-quality (LQ) ones. To compensate the information loss in the degradation process, prior knowledge of HQ image is indispensable. While deep neural networks (DNNs), especially Transformers for image restoration, have seen significant advancements in recent years, challenges still remain, particularly in the explicit incorporation of external priors, managing computational complexity, and tailoring generalized external priors to image specifics. To address these issues, we propose to enhance Transformer with **A**daptive **T**oken **D**ictionary (ATD), leading to a novel architecture which introduces a token dictionary to explicitly model external prior in the attention mechanism. The proposed ATD calculates the attention between the input features and the token dictionary, which integrates similar features on a global scale. Furthermore, we propose an adaptive dictionary refinement mechanism (ADR) to progressively customize the shared tokens to image specifics from shallow to deep layers. Crucially, benefiting from the condensed token dictionary, the computational complexity of the new attention mechanism is reduced from quadratic to linear with respect to the number of image tokens. This efficiency makes our network notably advantageous in constrained settings. Experimental results show that our method achieves best performance on various image restoration benchmark.

1 INTRODUCTION

The task of image restoration (IR) aims to recover clean high-quality (HQ) images from a solitary degraded low-quality (LQ) image or a sequence of such images, including image super-resolution, image denoising and JPEG compression artifact reduction. Since each LQ image may correspond to an infinite number of possible HQ images, image restoration is a classic ill-posed and challenging problem in the fields of computer vision and image processing. This practice is significant as it transcends the resolution and accuracy limitations of cost-effective sensors and enhances images produced by outdated equipment. The inherent information loss during the degradation process necessitates the incorporation of prior knowledge, specifically *external* and *internal* image priors, to supplement information for HQ image estimation. External priors refer to the generalized knowledge extracted from training datasets, whereas internal priors denote the image-specific information derived from the input image itself (Wang et al., 2015). The utilization and interplay of these external and internal image priors present numerous intriguing challenges and opportunities for exploration within the field.

In earlier research, various models such as Markov random field (He & Siu, 2011) and Dictionary Learning methods (Yang et al., 2010), were exploited to extract external priors explicitly from training datasets in a generative manner. The swift advancement of deep learning technologies in recent years has catalyzed an exponential increase in the application of deep neural network (DNN) models for image restoration. Pioneered by SRCNN (Dong et al., 2015) and DnCNN (Zhang et al., 2017a), convolutional neural network (CNN) based image restoration methods have emerged (Kim et al., 2016; Lim et al., 2017; Zhang et al., 2018a; Dai et al., 2020; Zhang et al., 2021). These methods directly learn the LQ-to-HQ mapping function with CNNs in a discriminative manner and implicitly embeds external prior knowledge of HQ image in the learned mapping functions. Recently, another family of DNNs, *i.e.*, Transformer-based image restoration networks have demonstrated their superiority to CNN-based networks, primarily by utilizing self-attention between image tokens to model internal image priors (Liang et al., 2021; Chen et al., 2023; Li et al., 2023). Yet, how to explicitly embed external priors in DNN-based solutions for image restoration remains to be answered.

The second highly related issue about modelling internal image priors with Transformer-based networks is the computational complexity. The size of receptive field in vision transformers plays a critical role in capturing internal prior across an extensive range of patches (Liu et al., 2021; 2022). Despite achievements in image partitioning for self-attention, it continues to grapple with escalating computational complexity, growing quadratically with the number of input tokens and quadruply with the window size, which becomes particularly evident with increased sizes (Chen et al., 2023).

Moreover, although external priors offer a broad understanding of various image characteristics and patterns, each image possesses unique features and nuances that cannot be fully captured by these generalized external priors. By tailoring these priors to the specifics of the individual image, the network can better understand and leverage the unique properties of that image, enhancing the quality and accuracy of the resultant HR image. This adaptive approach allows for a more personalized and precise image reconstruction.

In summary, we try to address the following three research questions in this paper:

1. What methods can be employed to explicitly integrate external image priors into Transformer-based networks?
2. How can we reduce the computational complexity of Transformer-based networks while effectively modeling internal image priors for image restoration?
3. How can we tailor the incorporated external image prior to specific image characteristics?

Our solution is inspired by the classical dictionary learning methods, which models image prior with learned dictionary items. We propose to learn and adapt a token dictionary which seamlessly solves the three research questions. First of all, the external prior of the entire training dataset is condensed into the token dictionary during the training process. To exploit the external prior of token dictionary, we then implement an attention operation to select relevant dictionary keys and reconstruct enhanced features with their corresponding value tokens. Secondly, the complexity of the above token dictionary attention mechanism (Vaswani et al., 2017) is notably reduced to linear in relation to the number of image tokens. This allows us to efficiently apply the attention mechanism to enhance all the tokens in the image. Thirdly, we propose a refining strategy to adaptively fit the public dictionary to specific testing image. Specifically, the the attention map between token dictionary and image tokens encapsulates the similarity relationship between image tokens and the dictionary. By recurrently weighting the enhanced token with previous attention map, we can refine the public token dictionary based on the enhanced local structures of the input image. When combined with the original Swin Multi-head Self-Attention (SW-MSA) block (Liu et al., 2021; Liang et al., 2021), our proposed Adaptive Token Dictionary Cross-Attention (ATDCA) block enables the proposed network to balance use of internal and external image prior effectively.

Our contributions can be summarized as follows:

- We introduce a token dictionary learning method that incorporates external prior from the training dataset to augment the internal prior of existing self-attention-based IR approaches.
- We put forward a cross-block refining strategy that adaptively tailors the learned public token dictionary to a specific input image during the testing phase, enhancing IR results.
- By combining the proposed adaptive token dictionary attention with Swin self-attention, we achieve a balanced use of internal and external priors. This proposed method offers an improved balance between accuracy and computational load compared with the current state-of-the-art.

2 Related Works

DNN-based Image Restoration. SRCNN (Dong et al., 2015) was the first to use deep learning for single image super-resolution with a simple 3-layer neural network. DnCNN (Zhang et al., 2017a) is a pioneering work in image denoising. Since its development, many other works (Kim et al., 2016; Lim et al., 2017; Zhang et al., 2018a; 2019; Dai et al., 2020; Niu et al., 2020; Mei et al., 2021; Zhang et al., 2021) have explored a vast range of structures to boost performance. Among them, EDSR (Lim et al., 2017) and RDN (Zhang et al., 2018b) introduced new residual blocks with detailed connection designs, enhancing the capabilities of convolutional neural networks further.

With the quick growth of Transformer (Vaswani et al., 2017) in NLP, several works have enhanced performance using attention mechanisms. Since ViT (Dosovitskiy et al., 2020) and its variants (Liu et al., 2021; Chu et al., 2021; Wang et al., 2022) have shown the effectiveness of pure Transformer-based models in image classification, more works are exploring the potential of Transformer-based networks (Liang et al., 2021; Zamir et al., 2022; Zhang et al., 2023; Chen et al., 2023; Li et al., 2023) in image restoration, showing their superiority to CNN-based methods. These studies investigated a range of techniques to enhance the performance of image restoration transformers. The explored methods include window self-attention (Liang et al., 2021), channel self-attention (Zamir et al., 2022), and anchored self-attention (Li et al., 2023), among others. Additionally, pretraining on extensive datasets (Li et al., 2021), employing sparse attention (Zhang et al., 2023), and utilizing large window sizes (Chen et al., 2023) were strategies used to further boost performance.

External Prior and Internal Prior Modeling. Image restoration is an ill-posed problem due to information loss during the degradation process. Additional knowledge is needed to compensate for the information loss. In earlier studies, some methods were proposed to estimate the HQ image using the Bayesian framework. But in the past two decades, most image restoration methods learn the LQ to HQ mapping directly, embedding the prior of HQ image in the learned mapping functions.

Traditionally, two types of prior have been used for image restoration (Wang et al., 2015). One approach learns an **external prior** from a universal set of training data to predict the missing information for the HR image. Various functions, including local regression models (Timofte et al., 2015), coupled dictionary learning models (Yang et al., 2010), and deep neural networks (Dong et al., 2015), have been used to capture the external prior implicitly. Another approach searches for example patches from the input image itself to use the image's internal prior of cross-scale non-local self-similarity (Freedman & Fattal, 2011; Glasner et al., 2009; Shocher et al., 2018), providing relevant but limited references.

Recently, besides using internal prior for mapping function learning, researchers also proposed using **internal prior** by designing specific network architectures. The non-local layer (Wang et al., 2018) in CNNs benefits from the non-local prior of natural images. The self-attention block (Dosovitskiy et al., 2020) uses similarity between input tokens to combine input token features effectively. Both the non-local block (Zhang et al., 2019) and the self-attention block (Liang et al., 2021) enhance CNNs or MLPs for image restoration by balancing the use of external and internal priors.

This paper reveals that the self-attention block in Vision Transformer (Dosovitskiy et al., 2020) can also effectively model external prior. Inspired by conventional dictionary learning approaches, we introduce token dictionaries to model image external prior explicitly in Transformer-based image restoration network. We propose an adaptive strategy that updates the token dictionary based on the specific content of the input image, balancing the use of internal and external prior and delivering state-of-the-art image restoration results.

3 Methodology

3.1 Motivation

In this subsection, we discuss how the dictionary learning based and self-attention based image restoration methods utilize external and internal prior to provide supplementary information for image restoration. Then we discuss how those two method motivates us to introduce external prior to Transformer-based methods with learned token dictionary.

Dictionary Learning for Image Restoration. Before the era of deep learning, dictionary learning methods play an important role in providing prior information for image restoration. Due to the limited computational resource, conventional dictionary learning based methods divide image into patches for modeling image local prior. Take image super-resolution for example. Denote $\boldsymbol{x} \in \mathbb{R}^d$ as a vectorized image patch in the low-resolution(LR) image. To estimate the corresponding high-resolution(HR) patch $\boldsymbol{y} \in \mathbb{R}^d$, Yang et al. (2010) decompose the signal by solving the sparse representation problem:

$$\boldsymbol{\alpha}^* = argmin_{\boldsymbol{\alpha}} \|\boldsymbol{x} - \boldsymbol{D}_L \boldsymbol{\alpha}\|_2^2 + \lambda \|\boldsymbol{\alpha}\|_1 \tag{1}$$

and reconstruct the HR patch with $\boldsymbol{D}_H \boldsymbol{\alpha}^*$; where $\boldsymbol{D}_L \in \mathbb{R}^{d \times N}$ and $\boldsymbol{D}_H \in \mathbb{R}^{d \times N}$ are the learned LR and HR dictionaries, and N is the number of atoms in the dictionary. The coupled dictionaries $\boldsymbol{D}_L$

and $\boldsymbol{D}_H$, summarize prior information of the external training dataset to compensate losing details in HR image.

Vision Transformer for Image Restoration. CNN-based image restoration methods learn spatially invariant convolution kernels from the training dataset to capture the LQ-to-HQ mapping. From a prior modeling perspective, local features of the input LQ image are enhanced based on external prior which were embedded in the convolution kernels in the training phase. On the other hand, the Transformer-based methods pay more attention to image internal priors and exploit similarity between tokens as weight to mutually enhance image features:

$$\text{Attention}(\boldsymbol{Q}, \boldsymbol{K}, \boldsymbol{V}) = \text{SoftMax}\left(\boldsymbol{Q}\boldsymbol{K}^T/\sqrt{d}\right)\boldsymbol{V}; \tag{2}$$

$\boldsymbol{Q} \in \mathbb{R}^{N\times d}$, $\boldsymbol{K} \in \mathbb{R}^{N\times d}$ and $\boldsymbol{V} \in \mathbb{R}^{N\times d}$ are linearly transformed from the input feature $\boldsymbol{X} \in \mathbb{R}^{N\times d}$ itself, N is the token number and d is the feature dimension. Due to the self-attentive processing philosophy, large window size plays a critical role in modeling internal prior of more patches. However, the complexity of self-attention computation increases quadratically with the number of input tokens, different strategies including shift-window (Liu et al., 2021; 2022; Liang et al., 2021; Conde et al., 2023), anchor attention (Li et al., 2023), and shifted crossed attention (Li et al., 2021) have been proposed to alleviate the limited window size issue of vision Transformer.

Token Dictionary: Empower Attention Block with External Prior. After reviewing the above contents, we found that the decomposition and reconstruction idea of dictionary learning based image restoration is similar to the process of self-attention computation. Specifically, the above method in Eq. 1 solves the sparse representation model to find similar LR dictionary atoms and reconstruct HR signal with the corresponding HR dictionary atoms; while the attention-based methods use normalized point product operation to determine attention values for combining value tokens. The above observation implies that the idea of using coupled dictionary $\boldsymbol{D}_L$ and $\boldsymbol{D}_H$ to introduce external prior can be easily incorporated into the Transformer framework. By learning an extra token dictionary instead of generating key and value tokens from input image, we can summarize external prior of training dataset for better restoration.

In the following sub-sections, we will firstly introduce how we design our Token Dictionary Cross-Attention (TDCA) block to introduce external prior into the Transformer framework. Then, we further improve our proposed TDCA by proposing a refine strategy to adaptively fit the public dictionary to each specific input image.

3.2 Token Dictionary Cross-Attention

In this subsection, we introduce details of our proposed token dictionary cross-attention block.

In comparison to the existing MSA which generates query, key and value tokens by the input feature itself. We aim to introduce an extra dictionary $\boldsymbol{D} \in \mathbb{R}^{M\times d}$ to summarize external prior from the training data. We use the learned token dictionary $\boldsymbol{D}$ to generate the Key Dictionary $\boldsymbol{K}_D$ and the Value Dictionary $\boldsymbol{V}_D$ and use the input feature $\boldsymbol{X} \in \mathbb{R}^{N\times d}$ to generate query tokens:

$$\boldsymbol{Q}_X = \boldsymbol{X}\boldsymbol{W}^Q, \qquad \boldsymbol{K}_D = \boldsymbol{D}\boldsymbol{W}^K, \qquad \boldsymbol{V}_D = \boldsymbol{D}\boldsymbol{W}^V, \tag{3}$$

where $M \ll N$, and $W^Q \in \mathbb{R}^{d\times d/r}$, $W^K \in \mathbb{R}^{d\times d/r}$ and $W^V \in \mathbb{R}^{d\times d}$ are linear transforms for Query Tokens, Key Dictionary Tokens and Value Dictionary Tokens, respectively. Note that the feature dimensions of query tokens and key dictionary tokens are reduced to $1/r$ for decreasing parameters and save computational resource consumption, where r is the reduction ratio. Then, we use the key dictionary and value dictionary to enhance query tokens via cross-attention calculation:

$$\text{TDCA}(\boldsymbol{Q}_X, \boldsymbol{K}_D, \boldsymbol{V}_D) = \text{SoftMax}\left(\boldsymbol{S}/\tau\right)\boldsymbol{V}_D, \quad \text{where } \boldsymbol{S} = \text{Sim}_{\cos}(\boldsymbol{Q}_X, \boldsymbol{K}_D). \tag{4}$$

In Eq. 4, τ is a learnable parameter for adjusting the range of similarity value. $\text{Sim}_{\cos}(\cdot,\cdot)$ represents calculating Cosine Similarity between two tokens, and $\boldsymbol{S} \in \mathbb{R}^{N\times M}$ is the similarity map between Query image tokens and Key dictionary tokens. We use the normalized Cosine distance instead of dot product operation in MSA because we want each token in the Dictionary to have equal opportunity to be selected, the similar magnitude normalization operation is commonly used in previous dictionary learning works.

The above TDCA operation firstly selects similar tokens in Key Dictionary tokens, which is similar to the sparse representation process in Eq. 1 to obtain representation coefficients; then, TDCA

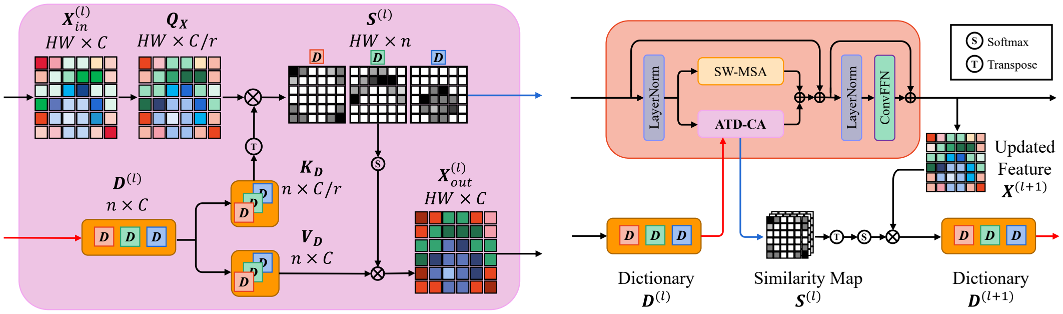

(a) Token Dictionary Cross-Attention

(b) Transformer Layer and Adaptive Dictionary Refinement

Figure 1: The proposed Token Dictionary Cross-Attention Block (TDCA) block and the Adaptive Dictionary Refinement (ADR) strategy. More details of our proposed TDCA and ADR can be found in Sec. 3.2 and 3.3, respectively.

utilizes the similarity values to combine the corresponding Value Dictionary tokens, which is the same as reconstructing HQ patch with HQ dictionary atoms and representation coefficients. By this way, our TDCA is able to embed the external prior into learned dictionary for enhancing the input image feature. We will validate the effectiveness of using token dictionary to provide external prior information in our ablation study at Sec. 4.1.

3.3 Adaptive Token Dictionary Refinement

In the previous subsection, we have presented how we could introduce an extra token dictionary to supply external prior for image restoration Transformer. Since the image feature in each block will be projected to different feature space by Multi-Layer Perceptrons (MLPs), we need to learn Token Dictionary for each block to provide external prior in each specific feature space. This will lead to a large number of extra parameters. In this subsection, we introduce an adaptive refining strategy which refines token dictionary of the previous block based on the similarity map and the updated features.

To introduce the proposed adaptive refining strategy, we set up the block index (l) for the input features and token dictionary, i.e. $\boldsymbol{X}^{(l)}$ and $\boldsymbol{D}^{(l)}$ denotes the input feature and token dictionary of the l-th block, respectively. We learn token dictionary for the first block $\boldsymbol{D}^{(0)}$ to introduce external prior as introduced in Sec. 3.2. While, for each token in the dictionary $\left\{\boldsymbol{d}_i^{(l)}\right\}_{i=1,\ldots,M}$ of the l-th block, we select the corresponding similar tokens in the image to refine it. To be more specific, we denote $\boldsymbol{s}_i^{(l-1)}$ as the i-th column of similarity map $\boldsymbol{S}^{(l-1)}$, it contains the distance between $\boldsymbol{d}_i^{(l-1)}$ and all the N query tokens $\boldsymbol{X}^{(l-1)}$. Therefore, based on $\boldsymbol{s}_i^{(l-1)}$, we are able to select the corresponding enhanced tokens $\boldsymbol{X}^{(l)}$ to reconstruct the new token dictionary $\boldsymbol{d}_i^{(l)}$:

$$\boldsymbol{D}^{(l)} = \mathrm{SoftMax}\left(\boldsymbol{S}^{(l-1)^T}/\sigma\right)\boldsymbol{X}^{(l)}, \tag{5}$$

where σ is a learnable scaling value to adjust the range of similarity map.

Thanks to the linear complexity of the proposed TDCA with the number of image tokens, we do not need to divide the image into windows and $\boldsymbol{X}^{(l)}$ represents all the image tokens. A visualization of the intermediate similarity map can be found in Fig. 2, it can be easily found that different similarity vectors $\boldsymbol{s}_i$ captures different types of textures in the input image. Starting from the initial token dictionary $\boldsymbol{D}^{(0)}$, which introduces external prior into the network, our adaptive refining strategy gradually select relevant tokens from the whole image to refine the dictionary. The refined dictionary could cross the boundary of self-attention window to summarize the typical local structures of the whole image, and consequently, improve image feature with global information.

3.4 The Overall Network Architecture

Having our proposed Token Dictionary Cross-Attention (TDCA) block and the Adaptive Dictionary Refinement (ADR) strategy in Sec. 3.2 and 3.3, we are able to establish our Adaptive Token Dictionary

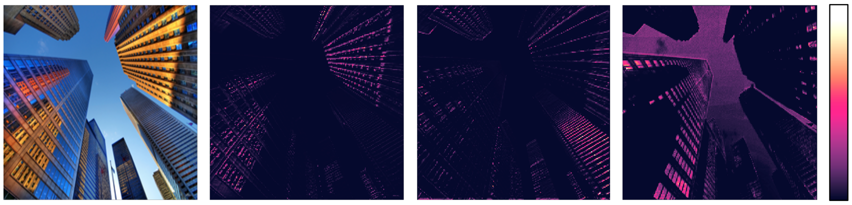

(a) (b) (c) (d)

Figure 2: Visualization of similarity vectors $\boldsymbol{s}_i^{(l)}$ of an image in the Urban 100 dataset. (b), (c) and (d) show similarity map between all the input tokens and three tokens in our token dictionary. The similarity map clearly shows that different tokens in the dictionary could detect different types of local structures. Therefore, we are able to adaptively fit the public dictionary to specific testing image by summarizing image structures based on the similarity map.

(ATD) network for image restoration. Given an input LQ image, we firstly utilize a 3×3 convolution layer to extract shallow features. Then, the shallow features are fed into several ATD blocks in specific architecture depending on the task. Each ATD block contains N_{Trans} transformer layers. The transformer layer contains our proposed Adaptive Token Dictionary Cross-Attention (ATDCA) and a Shift Window-based MSA(SW-MSA) (Liang et al., 2021; Liu et al., 2021), the two kinds of attention blocks process the input feature in parallel and the final features are combined by a summation operation. In addition to the attention block, our transformer layer also utilize LayerNorm and ConvFFN layers, which have been commonly utilized in other Transformer-based architectures. After the ATD blocks, we utilize an extra convolution layer (followed with pixel shuffle operation for SR task) to generate the final HQ estimation. For image SR, ATD blocks are connected in sequence and we provide an illustration of our network architecture in Fig. 3. For image denoising and JPEG compression artifact reduction, an encoder-decoder architecture is employed following previous works as shown in Fig. 6 in Appendix.

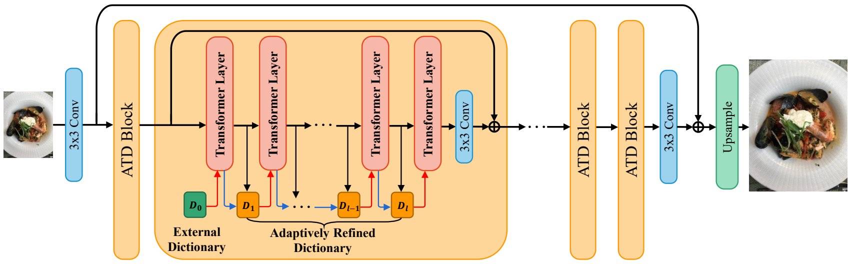

Figure 3: The overall architecture of the proposed ATD network for image super-resolution. The illustration of the ATD-U (encoder-decoder architecture for image denoising and JPEG compression artifact reduction) is presented in the Fig. 6.

4 Experiments

In this section we provide experimental results on several image restoration tasks including 1) image super-resolution, 2) image denoising, and 3) JPEG compression artifacts reduction. Three models with different architecture and parameter size are built for different tasks. We establish ATD as well as its tiny version ATD-light to tackle super-resolution problem, while ATD-U is designed for denoising and JPEG compression artifact reduction task. Due to page limitations, the detailed experimental settings are presented in the Appendix.

4.1 Ablation Study

Before comparing our model with state-of-the-art methods, we firstly conduct ablation studies to validate our design choices. We conduct ablation studies on re-scaled ATD-light model and train all the models for 500k iterations on DIV2K (Timofte et al., 2017) dataset. We then evaluate them on the Urban100 (Huang et al., 2015) benchmark.

Effects of External Token Dictionary and Adaptive Token Dictionary. In order to show the effectiveness of the proposed adaptive token dictionary cross-attention (ATDCA) approach, we establish three models and compare their capability for image SR. The first model is our final model **ATD**, which learns external token dictionary from training data and utilizes refinement strategy to update token dictionary in each ATD blocks. To demonstrate the effectiveness of learned token dictionary, we present a baseline model **ATD(-t)** which do not learn any token dictionary and only adopt SW-MSA block to process image features. Then, to analyze the effect of our adaptive dictionary refinement strategy, we establish another model, i.e. the **ATD(-a)**, which directly learns external token dictionary for each Transformer layer without applying adaptive refinement operation. The ablation results can be found in Table 1. The results clearly show that the learned token dictionary could provide external information for better SR, and the refinement strategy is able to further enhance the learned public dictionary while reducing the size of dictionary.

Table 1: Ablation study on the effects of each component. More details of the experimental settings can be found in our Ablation study section.

model	TD	ADR	PSNR(dB)	SSIM
ATD(-t)			26.67	0.8038
ATD(-a)	√		26.72	0.8044
ATD	√	√	26.77	0.8051

Table 2: Quantitative comparison (PSNR/SSIM) with state-of-the-art methods on **lightweight SR** and **classical SR** task. Best and second best results are colored with red and blue. More experimental details can be found in the main text.

Method	**Params**	**Scale**	**Set5**		**Set14**		**BSD100**		**Urban100**		**Manga109**	
			PSNR	SSIM	PSNR	SSIM	PSNR	SSIM	PSNR	SSIM	PSNR	SSIM
CARN (Ahn et al., 2018)	×2	1,592K	37.76	0.9590	33.52	0.9166	32.09	0.8978	31.92	0.9256	38.36	0.9765
IMDN (Hui et al., 2019)	×2	694K	38.00	0.9605	33.63	0.9177	32.19	0.8996	32.17	0.9283	38.88	0.9774
LAPAR-A (Li et al., 2020)	×2	548K	38.01	0.9605	33.62	0.9183	32.19	0.8999	32.10	0.9283	38.67	0.9772
LatticeNet (Luo et al., 2020)	×2	756K	38.15	0.9610	33.78	0.9193	32.25	0.9005	32.43	0.9302	-	-
SwinIR-light (Liang et al., 2021)	×2	910K	38.14	0.9611	33.86	0.9206	32.31	0.9012	32.76	0.9340	39.12	0.9783
ELAN (Zhang et al., 2022)	×2	582K	38.17	0.9611	33.94	0.9207	32.30	0.9012	32.76	0.9340	39.11	0.9782
SwinIR-NG (Choi et al., 2022)	×2	1181K	38.17	0.9612	33.94	0.9205	32.31	0.9013	32.78	0.9340	39.20	0.9781
OmniSR (Wang et al., 2023)	×2	772K	38.22	0.9613	33.98	0.9210	32.36	0.9020	33.05	0.9363	39.28	0.9784
ATD-light (ours)	×2	757K	38.27	0.9615	34.05	0.9218	32.38	0.9022	33.22	0.9380	39.35	0.9781
EDSR (Lim et al., 2017)	×2	42.6M	38.11	0.9602	33.92	0.9195	32.32	0.9013	32.93	0.9351	39.10	0.9773
RCAN (Zhang et al., 2018a)	×2	15.4M	38.27	0.9614	34.12	0.9216	32.41	0.9027	33.34	0.9384	39.44	0.9786
SAN (Dai et al., 2020)	×2	15.7M	38.31	0.9620	34.07	0.9213	32.42	0.9028	33.10	0.9370	39.32	0.9792
HAN (Niu et al., 2020)	×2	63.6M	38.27	0.9614	34.16	0.9217	32.41	0.9027	33.35	0.9385	39.46	0.9785
IPT (Chen et al., 2020)	×2	115M	38.37	-	34.43	-	32.48	-	33.76	-	-	-
SwinIR (Liang et al., 2021)	×2	11.8M	38.42	0.9623	34.46	0.9250	32.53	0.9041	33.81	0.9433	39.92	0.9797
EDT (Li et al., 2021)	×2	11.5M	38.45	0.9624	34.57	0.9258	32.52	0.9041	33.80	0.9425	39.93	0.9800
CAT-A (Chen et al., 2022)	×2	16.5M	38.51	0.9626	34.78	0.9265	32.59	0.9047	34.26	0.9440	40.10	0.9805
ART (Zhang et al., 2023)	×2	16.4M	38.56	0.9629	34.59	0.9267	32.58	0.9048	34.30	0.9452	40.24	0.9808
HAT (Chen et al., 2023)	×2	20.6M	38.63	0.9630	34.86	0.9274	32.62	0.9053	34.45	0.9466	40.26	0.9809
ATD (ours)	×2	18.7M	38.61	0.9630	34.77	0.9271	32.63	0.9054	34.49	0.9470	40.33	0.9808
CARN (Ahn et al., 2018)	×4	1,592K	32.13	0.8937	28.60	0.7806	27.58	0.7349	26.07	0.7837	30.47	0.9084
IMDN (Hui et al., 2019)	×4	715K	32.21	0.8948	28.58	0.7811	27.56	0.7353	26.04	0.7838	30.45	0.9075
LAPAR-A (Li et al., 2020)	×4	659K	32.15	0.8944	28.61	0.7818	27.61	0.7366	26.14	0.7871	30.42	0.9074
LatticeNet (Luo et al., 2020)	×4	777K	32.30	0.8962	28.68	0.7830	27.62	0.7367	26.25	0.7873	-	-
SwinIR-light (Liang et al., 2021)	×4	930K	32.44	0.8976	28.77	0.7858	27.69	0.7406	26.47	0.7980	30.92	0.9151
ELAN (Zhang et al., 2022)	×4	582K	32.43	0.8975	28.78	0.7858	27.69	0.7406	26.54	0.7982	30.92	0.9150
SwinIR-NG (Choi et al., 2022)	×4	1201K	32.44	0.8980	28.83	0.7870	27.73	0.7418	26.61	0.8010	31.09	0.9161
OmniSR (Wang et al., 2023)	×4	792K	32.49	0.8988	28.78	0.7859	27.71	0.7415	26.65	0.8018	31.02	0.9151
ATD-light (ours)	×4	772K	32.50	0.8988	28.86	0.7884	27.76	0.7431	26.89	0.8097	31.29	0.9184
EDSR (Lim et al., 2017)	×4	43.0M	32.46	0.8968	28.80	0.7876	27.71	0.7420	26.64	0.8033	31.02	0.9148
RCAN (Zhang et al., 2018a)	×4	15.6M	32.63	0.9002	28.87	0.7889	27.77	0.7436	26.82	0.8087	31.22	0.9173
SAN (Dai et al., 2020)	×4	15.9M	32.64	0.9003	28.92	0.7888	27.78	0.7436	26.79	0.8068	31.18	0.9169
HAN (Niu et al., 2020)	×4	64.2M	32.64	0.9002	28.90	0.7890	27.80	0.7442	26.85	0.8094	31.42	0.9177
IPT (Chen et al., 2020)	×4	116M	32.64	-	29.01	-	27.82	-	27.26	-	-	-
SwinIR (Liang et al., 2021)	×4	11.9M	32.92	0.9044	29.09	0.7950	27.92	0.7489	27.45	0.8254	32.03	0.9260
EDT (Li et al., 2021)	×4	11.6M	32.82	0.9031	29.09	0.7939	27.91	0.7483	27.46	0.8246	32.05	0.9254
CAT-A (Chen et al., 2022)	×4	16.6M	33.08	0.9052	29.18	0.7960	27.99	0.7510	27.89	0.8339	32.39	0.9285
ART (Zhang et al., 2023)	×4	16.6M	33.04	0.9051	29.16	0.7958	27.97	0.7510	27.77	0.8321	32.31	0.9283
HAT (Chen et al., 2023)	×4	20.8M	33.04	0.9056	29.23	0.7973	28.00	0.7517	27.97	0.8368	32.48	0.9292
ATD (ours)	×4	18.9M	33.07	0.9061	29.20	0.7979	28.01	0.7518	27.98	0.8374	32.49	0.9292

4.2 Image Super-Resolution

We firstly evaluate the proposed ATD method on the image super-resolution task. We choose Set5 (Bevilacqua et al., 2012), Set14 (Zeyde et al., 2012), BSD100 (Martin et al., 2002), Urban100 (Huang et al., 2015), and Manga109 (Matsui et al., 2016) as evaluation datasets and compare with recent state-of-the-art SR methods. For the task of lightweight SR, we compare our method with CARN (Ahn et al., 2018), IMDN (Hui et al., 2019), LAPAR (Li et al., 2020), LatticeNet (Luo et al., 2020), SwinIR (Liang et al., 2021), ELAN (Zhang et al., 2022) and OmniSR (Wang et al., 2023).

As can be found in Table 2, the proposed ATD-light achieved better results with OmniSR (Wang et al., 2023) in both ×2 and ×4 zooming factors across most of benchmark datasets. Our ATD-light outperform recently proposed light-weight method OmniSR by a large margin (0.27dB) on the anga109 dataset. e believe this is because more information was lost during the downscaling process for cases with large zoom factors. With the learned and refined token dictionary, our ATD-light model is able to make better use of external prior for recovering HR details in challenging conditions.

We further compare our method with state-of-the-art SR methods: EDSR (Lim et al., 2017), RCAN (Zhang et al., 2018a), SAN (Dai et al., 2020), HAN (Niu et al., 2020), CSNLN (Mei et al., 2020), IPT (Chen et al., 2020), SwinIR (Liang et al., 2021), CAT (Chen et al., 2022), ART (Zhang et al., 2023), HAT (Chen et al., 2023). With about 10% less number of parameters(18.7M vs. 20.8M), the proposed ATD model still outperforms HAT (Chen et al., 2023). We achieved +0.07dB PSNR gain on the ×2 Manga109 dataset.

Some visual examples by different methods can be found in Fig. 4. The images in Fig. 4 clearly demonstrate our advantages in recovering sharp edges and clean textures. More visual examples can be found in the Appendix A.3.

Table 3: Quantitative comparison (PSNR) with state-of-the-art methods on **grayscale image denoising**. Best and second best results are colored with red and blue. More experimental details can be found in the main text.

Dataset	σ	BM3D	DnCNN	IRCNN	RNAN	RDN	DRUNet	SwinIR	Restormer	**ATD-U** (ours)
Set12	15	32.37	32.86	32.76	-	-	33.25	33.36	33.42	33.47
	25	29.97	30.44	30.37	-	-	30.94	31.01	31.08	31.16
	50	26.72	27.18	27.12	27.70	27.60	27.90	27.91	28.00	28.09
BSD68	15	31.08	31.73	31.63	-	-	31.91	31.97	31.96	31.97
	25	28.57	29.23	29.15	-	-	29.48	29.50	29.52	29.51
	50	25.60	26.23	26.19	26.48	26.41	26.59	26.58	26.62	26.54
Urban100	15	32.35	32.64	32.46	-	-	33.44	33.70	33.79	34.05
	25	29.70	29.95	29.80	-	-	31.11	31.30	31.46	31.83
	50	25.95	26.26	26.22	27.65	27.40	27.96	27.98	28.29	28.81

4.3 Image Denoising

We build ATD-U based on encoder-decoder architecture following Zamir et al. (2022) for grayscale image denoising task and make comparison with recent state-of-the-art methods: DnCNN (Zhang et al., 2017a), IRCNN (Zhang et al., 2017b), RNAN (Zhang et al., 2019), RDN (Zhang et al., 2018b), DRUNet (Zhang et al., 2021), SwinIR (Liang et al., 2021), Restormer (Zamir et al., 2022) on Set12 (Zhang et al., 2017a), BSD68 (Martin et al., 2001) and Urban100 (Huang et al., 2015) datasets.

The quantitative results are shown in Table 3. Our ATD-U outperforms Restormer by a large margin up to 0.52dB on Urban100 benchmark under challenging noise level of 50 with 10% smaller model size (23.5M) compared to Restormer(26.1M). These comparisons illustrate the strong power of external prior when restoring image from severe noise. ATD-U also exhibits comparable and better performance on BSD68 and other datasets. These results indicate the powerful capacity of ATD-U to mitigate noise in grayscale images. We provide some visual examples in Fig. 4. These comparisons illustrate that ATD-U possess the ability to restore cleaner image from heavy noise pollution while resulting in less artifacts. More visual comparisons can be found in the Appendix A.3.

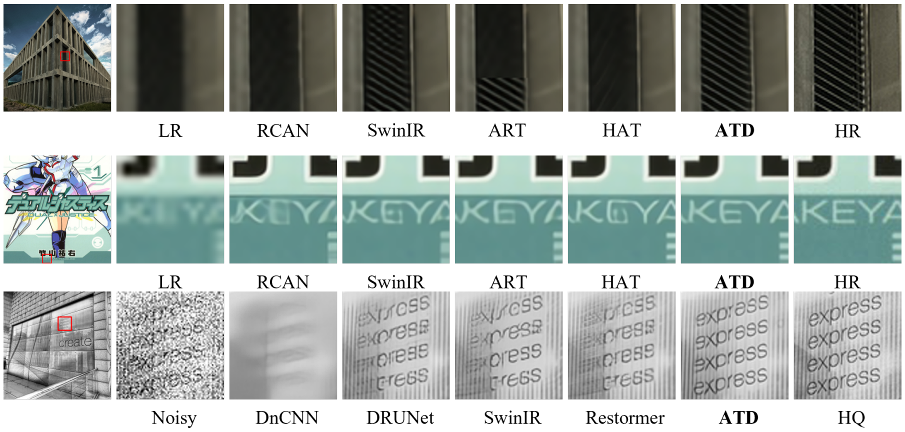

Figure 4: Visual comparisons of **image super-resolution** methods on image Urban100-"img027", Manga109-"DualJustice" and **grayscale image denoising** methods on image Urban100-"img060"

4.4 JPEG Compression Artifact Reduction

Same as image denoising task, we employ ATD-U model on JPEG compression artifact reduction task and make comparison with recent state-of-the-art methods: DnCNN (Zhang et al., 2017a), RNAN (Zhang et al., 2019), RDN (Zhang et al., 2018b), DRUNet (Zhang et al., 2021), SwinIR (Liang et al., 2021), ART (Zhang et al., 2023). We choose Classic5 (Foi et al., 2007), LIVE1 (Sheikh et al., 2006) and Urban100 (Huang et al., 2015) as evaluation datasets. The experimental results are presented in Table 4. Our ATD-U achieves better performance compared to previous methods SwinIR and ART. ATD-U obtains up to 0.25dB gain on Urban100 under challenging compression quality factor(QF=10). These results manifest that ATD-U also has strong artifact removal ability for JPEG compression artifact reduction.

Table 4: Quantitative comparison (PSNR/SSIM) with state-of-the-art methods on **JPEG compression artifact reduction**. Best and second best results are colored with red and blue. More experimental details can be found in the main text.

Set	QF	Grayscale										Set	QF	Color					
		DnCNN		DRUNet		SwinIR		ART		**ATD-U** (ours)				DRUNet		SwinIR		**ATD-U** (ours)	
		PSNR	SSIM	PSNR	SSIM	PSNR	SSIM	PSNR	SSIM	PSNR	SSIM			PSNR	SSIM	PSNR	SSIM	PSNR	SSIM
Classic5	10	29.40	0.8013	30.16	0.8234	30.27	0.8249	30.27	0.8258	30.38	0.8272	**Classic5**	10	27.47	0.8045	28.06	0.8129	28.32	0.8179
	20	31.63	0.8596	32.39	0.8734	32.52	0.8748	-	-	32.60	0.8751		20	30.29	0.8743	30.44	0.8768	30.58	0.8787
	30	32.91	0.8855	33.59	0.8949	33.73	0.8961	33.74	0.8964	33.80	0.8962		30	31.64	0.9020	31.81	0.9040	31.97	0.9059
	40	33.77	0.8993	34.41	0.9075	34.52	0.9082	34.55	0.9086	34.59	0.9082		40	32.56	0.9174	32.75	0.9193	32.89	0.9205
LIVE1	10	29.19	0.8172	29.79	0.8278	29.86	0.8287	29.89	0.8300	29.94	0.8371	**BSD500**	10	27.62	0.8001	28.22	0.8075	28.32	0.8083
	20	31.59	0.8848	32.17	0.8899	32.25	0.8909	-	-	32.31	0.8949		20	30.39	0.8711	30.54	0.8739	30.54	0.8730
	30	32.98	0.9167	33.59	0.9166	33.69	0.9174	33.71	0.9178	33.72	0.9226		30	31.73	0.9003	31.90	0.9025	31.90	0.9020
	40	33.96	0.9294	34.58	0.9312	34.67	0.9317	34.70	0.9322	34.70	0.9342		40	32.66	0.9168	32.84	0.9189	32.80	0.9178
Urban100	10	28.54	0.8484	30.31	0.8745	30.55	0.8835	30.87	0.8894	31.12	0.8935	**Urban100**	10	27.10	0.8400	28.18	0.8586	29.07	0.8726
	20	31.01	0.9050	32.81	0.9241	33.12	0.9190	-	-	33.52	0.9271		20	30.17	0.8991	30.53	0.9030	31.14	0.9094
	30	32.47	0.9312	34.23	0.9414	34.58	0.9417	34.81	0.9442	34.85	0.9458		30	31.49	0.9189	31.87	0.9219	32.48	0.9271
	40	33.49	0.9412	35.20	0.9547	35.50	0.9515	35.73	0.9553	35.73	0.9573		40	32.36	0.9301	32.75	0.9329	33.27	0.9365

4.5 Computational burden analysis

We further analyze the computational burden of the proposed ATD model. In Fig. 5, we present the image restoration accuracy (PSNR) and computational consumption of recent state-of-the-art models on the image SR and denoising tasks. The figures clearly demonstrate that the proposed ATD model helps the network to achieve a better trade-off between restoration accuracy and efficiency. Our ATD method achieves better SR results with 10% and 50% less computations than the HAT and ART model, respectively. Moreover, with only 10% more computations, our ATD-U model is able to improve the denoising performance of Restormer by a large margin (0.52dB). In comparison with the baseline SwinIR approach, ATD-U surpasses SwinIR by 0.83dB with 3.7× less FLOPs.

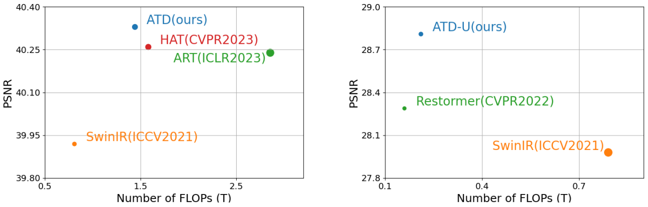

Figure 5: Comparison of PSNR and FLOPs by our model and S.O.T.A approaches (SR: Manga109 $\times$ 2; Denoise: Urban100 $\sigma = 50$), FLOPs are calculated on input size of 256×256.

5 Conclusion

In this paper, we proposed a new Transformer-based image restoration network. Inspired by the traditional dictionary learning methods, we proposed to learn token dictionaries to provide external supplementary information for estimating the missing high-quality details. We further proposed an adaptive dictionary refinement strategy which could use similarity map of the previous block to refine the externally learned dictionary, making it better fit the content of specific input image. We conducted ablation studies to demonstrate the effectiveness of the proposed token dictionary and adaptive refinement strategy. Extensive experimental results on plenty of benchmark datasets have been presented, our method achieved state-of-the-art results on image super-resolution, grayscale image denoising and JPEG compression artifact reduction.

REFERENCES

Namhyuk Ahn, Byungkon Kang, and Kyung-Ah Sohn. Fast, accurate, and lightweight super-resolution with cascading residual network, Mar 2018.

Pablo Arbelaez, Michael Maire, Charless Fowlkes, and Jitendra Malik. Contour detection and hierarchical image segmentation. *IEEE Trans. Pattern Anal. Mach. Intell.*, 33(5):898–916, May 2011. ISSN 0162-8828. doi: 10.1109/TPAMI.2010.161. URL http://dx.doi.org/10.1109/TPAMI.2010.161.

Marco Bevilacqua, Aline Roumy, Christine Guillemot, and Marie-line Alberi Morel. Low-complexity single-image super-resolution based on nonnegative neighbor embedding. In *Procedings of the British Machine Vision Conference 2012*, Sep 2012. doi: 10.5244/c.26.135. URL http://dx.doi.org/10.5244/c.26.135.

Hanting Chen, Yunhe Wang, Tianyu Guo, Chang Xu, Yiping Deng, Zhenhua Liu, Siwei Ma, Chunjing Xu, Chao Xu, and Wen Gao. Pre-trained image processing transformer, Dec 2020.

Xiangyu Chen, Xintao Wang, Jiantao Zhou, Yu Qiao, and Chao Dong. Activating more pixels in image super-resolution transformer. In *Proceedings of the IEEE/CVF Conference on Computer Vision and Pattern Recognition (CVPR)*, pp. 22367–22377, June 2023.

Zheng Chen, Yulun Zhang, Jinjin Gu, Yongbing Zhang, Linghe Kong, and Xin Yuan. Cross aggregation transformer for image restoration. In *NeurIPS*, 2022.

Haram Choi, Jeongmin Lee, and Jihoon Yang. N-gram in swin transformers for efficient lightweight image super-resolution, Nov 2022.

Xiangxiang Chu, Zhi Tian, Yuqing Wang, Bo Zhang, Haibing Ren, Xiaolin Wei, Huaxia Xia, and Chunhua Shen. Twins: Revisiting the design of spatial attention in vision transformers, Dec 2021.

Marcos V Conde, Ui-Jin Choi, Maxime Burchi, and Radu Timofte. Swin2sr: Swinv2 transformer for compressed image super-resolution and restoration. In *Computer Vision–ECCV 2022 Workshops: Tel Aviv, Israel, October 23–27, 2022, Proceedings, Part II*, pp. 669–687. Springer, 2023.

Tao Dai, Jianrui Cai, Yongbing Zhang, Shu-Tao Xia, and Lei Zhang. Second-order attention network for single image super-resolution. In *2019 IEEE/CVF Conference on Computer Vision and Pattern Recognition (CVPR)*, Jan 2020. doi: 10.1109/cvpr.2019.01132. URL http://dx.doi.org/10.1109/cvpr.2019.01132.

Jia Deng, Wei Dong, Richard Socher, Li-Jia Li, Kai Li, and Li Fei-Fei. Imagenet: A large-scale hierarchical image database. In *2009 IEEE conference on computer vision and pattern recognition*, pp. 248–255. Ieee, 2009.

Chao Dong, Chen Change Loy, Kaiming He, and Xiaoou Tang. Image super-resolution using deep convolutional networks. *IEEE Transactions on Pattern Analysis and Machine Intelligence*, pp. 295–307, Jun 2015. doi: 10.1109/tpami.2015.2439281. URL http://dx.doi.org/10.1109/tpami.2015.2439281.

Alexey Dosovitskiy, Lucas Beyer, Alexander Kolesnikov, Dirk Weissenborn, Xiaohua Zhai, Thomas Unterthiner, Mostafa Dehghani, Matthias Minderer, Georg Heigold, Sylvain Gelly, Jakob Uszkoreit, and Neil Houlsby. An image is worth 16x16 words: Transformers for image recognition at scale, Oct 2020.

Alessandro Foi, Vladimir Katkovnik, and Karen Egiazarian. Pointwise shape-adaptive dct for high-quality denoising and deblocking of grayscale and color images. *IEEE transactions on image processing*, 16(5):1395–1411, 2007.

Rich Franzen. Kodak lossless true color image suite. https://r0k.us/graphics/kodak/, 1999.

Gilad Freedman and Raanan Fattal. Image and video upscaling from local self-examples. *ACM Transactions on Graphics (TOG)*, 30(2):1–11, 2011.

Daniel Glasner, Shai Bagon, and Michal Irani. Super-resolution from a single image. In *2009 IEEE 12th international conference on computer vision*, pp. 349–356. IEEE, 2009.

He He and Wan-Chi Siu. Single image super-resolution using gaussian process regression. In *CVPR 2011*, pp. 449–456. IEEE, 2011.

Jia-Bin Huang, Abhishek Singh, and Narendra Ahuja. Single image super-resolution from transformed self-exemplars. In *2015 IEEE Conference on Computer Vision and Pattern Recognition (CVPR)*, Oct 2015. doi: 10.1109/cvpr.2015.7299156. URL http://dx.doi.org/10.1109/cvpr.2015.7299156.

Zheng Hui, Xinbo Gao, Yunchu Yang, and Xiumei Wang. Lightweight image super-resolution with information multi-distillation network. In *Proceedings of the 27th ACM International Conference on Multimedia*, Oct 2019. doi: 10.1145/3343031.3351084. URL http://dx.doi.org/10.1145/3343031.3351084.

Jiwon Kim, Jung Kwon Lee, and Kyoung Mu Lee. Accurate image super-resolution using very deep convolutional networks. In *2016 IEEE Conference on Computer Vision and Pattern Recognition (CVPR)*, Dec 2016. doi: 10.1109/cvpr.2016.182. URL http://dx.doi.org/10.1109/cvpr.2016.182.

Wenbo Li, Kun Zhou, Lu Qi, Nianjuan Jiang, Jiangbo Lu, and Jiaya Jia. Lapar: Linearly-assembled pixel-adaptive regression network for single image super-resolution and beyond, Jan 2020.

Wenbo Li, Xin Lu, Jiangbo Lu, Xiangyu Zhang, and Jiaya Jia. On efficient transformer and image pre-training for low-level vision. *arXiv preprint arXiv:2112.10175*, 2021.

Yawei Li, Yuchen Fan, Xiaoyu Xiang, Denis Demandolx, Rakesh Ranjan, Radu Timofte, and Luc Van Gool. Efficient and explicit modelling of image hierarchies for image restoration. In *Proceedings of the IEEE Conference on Computer Vision and Pattern Recognition*, 2023.

Jingyun Liang, Jiezhang Cao, Guolei Sun, Kai Zhang, Luc Van Gool, and Radu Timofte. Swinir: Image restoration using swin transformer, 2021.

Bee Lim, Sanghyun Son, Heewon Kim, Seungjun Nah, and Kyoung Mu Lee. Enhanced deep residual networks for single image super-resolution. In *2017 IEEE Conference on Computer Vision and Pattern Recognition Workshops (CVPRW)*, Aug 2017. doi: 10.1109/cvprw.2017.151. URL http://dx.doi.org/10.1109/cvprw.2017.151.

Ze Liu, Yutong Lin, Yue Cao, Han Hu, Yixuan Wei, Zheng Zhang, Stephen Lin, and Baining Guo. Swin transformer: Hierarchical vision transformer using shifted windows, 2021.

Ze Liu, Han Hu, Yutong Lin, Zhuliang Yao, Zhenda Xie, Yixuan Wei, Jia Ning, Yue Cao, Zheng Zhang, Li Dong, et al. Swin transformer v2: Scaling up capacity and resolution. In *Proceedings of the IEEE/CVF conference on computer vision and pattern recognition*, pp. 12009–12019, 2022.

Ilya Loshchilov and Frank Hutter. Sgdr: Stochastic gradient descent with warm restarts. In *International Conference on Learning Representations*, 2016.

Ilya Loshchilov and Frank Hutter. Decoupled weight decay regularization. In *International Conference on Learning Representations*, 2018.

Xiaotong Luo, Yuan Xie, Yulun Zhang, Yanyun Qu, Cuihua Li, and Yun Fu. *LatticeNet: Towards Lightweight Image Super-Resolution with Lattice Block*, pp. 272–289. Nov 2020. doi: 10.1007/978-3-030-58542-6_17. URL http://dx.doi.org/10.1007/978-3-030-58542-6_17.

Kede Ma, Zhengfang Duanmu, Qingbo Wu, Zhou Wang, Hongwei Yong, Hongliang Li, and Lei Zhang. Waterloo Exploration Database: New challenges for image quality assessment models. *IEEE Transactions on Image Processing*, 26(2):1004–1016, Feb. 2017.

D. Martin, C. Fowlkes, D. Tal, and J. Malik. A database of human segmented natural images and its application to evaluating segmentation algorithms and measuring ecological statistics. In *Proc. 8th Int'l Conf. Computer Vision*, volume 2, pp. 416–423, July 2001.

D. Martin, C. Fowlkes, D. Tal, and J. Malik. A database of human segmented natural images and its application to evaluating segmentation algorithms and measuring ecological statistics. In *Proceedings Eighth IEEE International Conference on Computer Vision. ICCV 2001*, Nov 2002. doi: 10.1109/iccv.2001.937655. URL http://dx.doi.org/10.1109/iccv.2001.937655.

Yusuke Matsui, Kota Ito, Yuji Aramaki, Azuma Fujimoto, Toru Ogawa, Toshihiko Yamasaki, and Kiyoharu Aizawa. Sketch-based manga retrieval using manga109 dataset. *Multimedia Tools and Applications*, pp. 21811–21838, Nov 2016. doi: 10.1007/s11042-016-4020-z. URL http://dx.doi.org/10.1007/s11042-016-4020-z.

Yiqun Mei, Yuchen Fan, Yuqian Zhou, Lichao Huang, Thomas S Huang, and Humphrey Shi. Image super-resolution with cross-scale non-local attention and exhaustive self-exemplars mining. In *Proceedings of the IEEE Conference on Computer Vision and Pattern Recognition (CVPR)*, 2020.

Yiqun Mei, Yuchen Fan, and Yuqian Zhou. Image super-resolution with non-local sparse attention. In *2021 IEEE/CVF Conference on Computer Vision and Pattern Recognition (CVPR)*, Nov 2021. doi: 10.1109/cvpr46437.2021.00352. URL http://dx.doi.org/10.1109/cvpr46437.2021.00352.

Ben Niu, Weilei Wen, Wenqi Ren, Xiangde Zhang, Lianping Yang, Shuzhen Wang, Kaihao Zhang, Xiaochun Cao, and Haifeng Shen. *Single Image Super-Resolution via a Holistic Attention Network*, pp. 191–207. Oct 2020. doi: 10.1007/978-3-030-58610-2_12. URL http://dx.doi.org/10.1007/978-3-030-58610-2_12.

Hamid R Sheikh, Muhammad F Sabir, and Alan C Bovik. A statistical evaluation of recent full reference image quality assessment algorithms. *IEEE Transactions on image processing*, 15(11): 3440–3451, 2006.

Assaf Shocher, Nadav Cohen, and Michal Irani. "zero-shot" super-resolution using deep internal learning. In *Proceedings of the IEEE conference on computer vision and pattern recognition*, pp. 3118–3126, 2018.

Radu Timofte, Vincent De Smet, and Luc Van Gool. A+: Adjusted anchored neighborhood regression for fast super-resolution. In *Computer Vision–ACCV 2014: 12th Asian Conference on Computer Vision, Singapore, Singapore, November 1-5, 2014, Revised Selected Papers, Part IV 12*, pp. 111–126. Springer, 2015.

Radu Timofte, Eirikur Agustsson, Luc Van Gool, Ming-Hsuan Yang, Lei Zhang, Bee Lim, Sanghyun Son, Heewon Kim, Seungjun Nah, Kyoung Mu Lee, et al. Ntire 2017 challenge on single image super-resolution: Methods and results. In *2017 IEEE Conference on Computer Vision and Pattern Recognition Workshops (CVPRW)*, Aug 2017. doi: 10.1109/cvprw.2017.149. URL http://dx.doi.org/10.1109/cvprw.2017.149.

Ashish Vaswani, Noam Shazeer, Niki Parmar, Jakob Uszkoreit, Llion Jones, Aidan N. Gomez, Lukasz Kaiser, and Illia Polosukhin. Attention is all you need, 2017.

Hang Wang, Xuanhong Chen, Bingbing Ni, Yutian Liu, and Liu jinfan. Omni aggregation networks for lightweight image super-resolution. In *Conference on Computer Vision and Pattern Recognition*, 2023.

Wenhai Wang, Enze Xie, Xiang Li, Deng-Ping Fan, Kaitao Song, Ding Liang, Tong Lu, Ping Luo, and Ling Shao. Pyramid vision transformer: A versatile backbone for dense prediction without convolutions. In *2021 IEEE/CVF International Conference on Computer Vision (ICCV)*, Mar 2022. doi: 10.1109/iccv48922.2021.00061. URL http://dx.doi.org/10.1109/iccv48922.2021.00061.

Xiaolong Wang, Ross Girshick, Abhinav Gupta, and Kaiming He. Non-local neural networks. In *Proceedings of the IEEE conference on computer vision and pattern recognition*, pp. 7794–7803, 2018.

Zhangyang Wang, Yingzhen Yang, Zhaowen Wang, Shiyu Chang, Jianchao Yang, and Thomas S Huang. Learning super-resolution jointly from external and internal examples. *IEEE Transactions on Image Processing*, 24(11):4359–4371, 2015.

Jianchao Yang, John Wright, Thomas S Huang, and Yi Ma. Image super-resolution via sparse representation. *IEEE transactions on image processing*, 19(11):2861–2873, 2010.

Syed Waqas Zamir, Aditya Arora, Salman Khan, Munawar Hayat, Fahad Shahbaz Khan, and Ming-Hsuan Yang. Restormer: Efficient transformer for high-resolution image restoration. In *CVPR*, 2022.

Roman Zeyde, Michael Elad, and Matan Protter. *On Single Image Scale-Up Using Sparse-Representations*, pp. 711–730. Jan 2012. doi: 10.1007/978-3-642-27413-8_47. URL http://dx.doi.org/10.1007/978-3-642-27413-8_47.

Jiale Zhang, Yulun Zhang, Jinjin Gu, Yongbing Zhang, Linghe Kong, and Xin Yuan. Accurate image restoration with attention retractable transformer. In *ICLR*, 2023.

Kai Zhang, Wangmeng Zuo, Yunjin Chen, Deyu Meng, and Lei Zhang. Beyond a Gaussian denoiser: Residual learning of deep CNN for image denoising. *IEEE Transactions on Image Processing*, 26 (7):3142–3155, 2017a.

Kai Zhang, Wangmeng Zuo, Shuhang Gu, and Lei Zhang. Learning deep cnn denoiser prior for image restoration. In *IEEE Conference on Computer Vision and Pattern Recognition*, pp. 3929–3938, 2017b.

Kai Zhang, Yawei Li, Wangmeng Zuo, Lei Zhang, Luc Van Gool, and Radu Timofte. Plug-and-play image restoration with deep denoiser prior. *IEEE Transactions on Pattern Analysis and Machine Intelligence*, 44(10):6360–6376, 2021.

Xindong Zhang, Hui Zeng, Shi Guo, and Lei Zhang. Efficient long-range attention network for image super-resolution. In *European Conference on Computer Vision*, 2022.

Yulun Zhang, Kunpeng Li, Kai Li, Lichen Wang, Bineng Zhong, and Yun Fu. *Image Super-Resolution Using Very Deep Residual Channel Attention Networks*, pp. 294–310. Oct 2018a. doi: 10.1007/978-3-030-01234-2_18. URL http://dx.doi.org/10.1007/978-3-030-01234-2_18.

Yulun Zhang, Yapeng Tian, Yu Kong, Bineng Zhong, and Yun Fu. Residual dense network for image super-resolution, Feb 2018b.

Yulun Zhang, Kunpeng Li, Kai Li, Bineng Zhong, and Yun Fu. Residual non-local attention networks for image restoration. In *ICLR*, 2019.

A Appendix

A.1 Experimental setting details.

A.1.1 Network architecture setting.

ATD For image super-resolution task, we establish ATD model that employs a sequence of ATD blocks as its backbone. There are 6 ATD blocks in total, each comprising six transformer layers with a channel number of 200. We establish 512 external tokens for our dictionary in ATD model and use a reduction rate r of 10. Each external token has 200 feature dimensions as in the SW-MSA branch, and each external token dictionary is randomly initialized as a tensor with shape of $[512, 200]$ in normal distribution.

ATD-light ATD-light is a tiny version of ATD which reduce feature dimensions to 48 for lightweight SR task. The number of dictionary token is decreased to 64 and we also adjust the reduction rate r to 4 for keeping enough in similarity calculation.

ATD-U For image denoising and JPEG compression artifact reduction, we employ a 4-level encoder-decoder architecture on ATD-U following Restormer (Zamir et al., 2022). An illustration of ATD-U architecture is presented in Fig. 6. We set the number of Transformer layers for each level as [4, 6, 6, 8], while the number of channel and reduction rate r are set as [48, 96, 192, 384] and [3, 6, 12, 24]. The parameter setting of refinement block is the same as level-1 encoder.

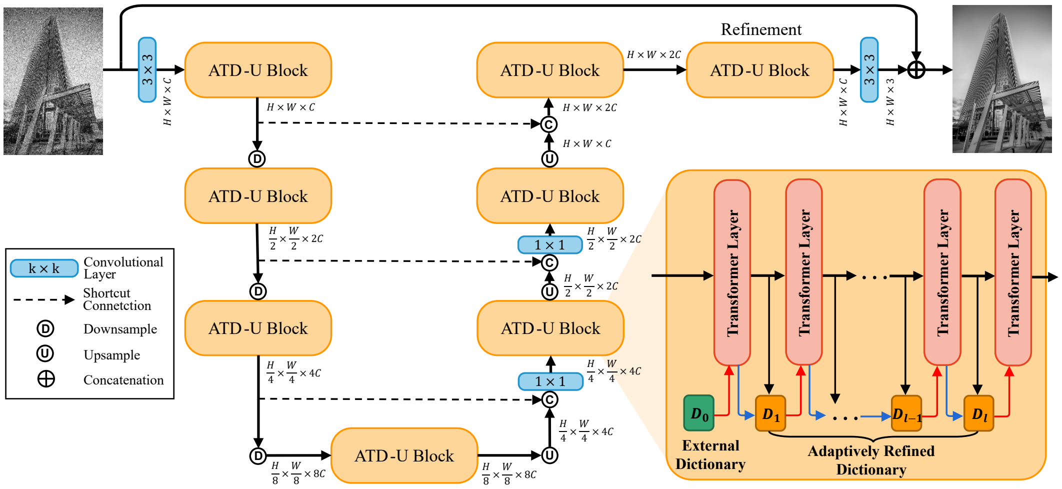

Figure 6: The overall architecture of the proposed ATD-U network for image denoising and JPEG compression artifact reduction.

A.1.2 Other details about architecture.

Hard threshold operation. When applying adaptive token dictionary refinement as mentioned in Eq. 5, we combine the similarity map and features to generate refined token dictionary. Practically, instead of directly using the similarity map from the previous block, we adopt an additional hard thresholding operation:

$$\boldsymbol{S}_\delta(i,j) = \mathrm{HardThresholding}\left(\boldsymbol{S}(i,j);\delta\right) = \begin{cases} \boldsymbol{S}(i,j) & \text{if } \boldsymbol{S}(i,j) \geq \delta \\ -\infty & \text{if } \boldsymbol{S}(i,j) < \delta \end{cases}, \tag{6}$$

where δ is the threshold in the hard thresholding operator and $-\infty$ is set to a small enough number to ensure that the value after Softmax is 0. Adopting $\boldsymbol{S}_\delta^{(l)}$ instead of $\boldsymbol{S}^{(l)}$ in Eq. 5 enables us to filter out irrelevant tokens with small similarity values and only use highly similar image tokens to update the tokens in the token dictionary.

ConvFFN. Recently, several works such as Zamir et al. (2022) start to add depth-wise convolutional layers and gating mechanism into feed-forward network. We simply adopt depth-wise convolution between two linear layers in FFN. It yields obvious improvement on ATD-light but little to ATD, since the extra receptive field brought by DWConv has a greater impact on shallow networks. The kernel size of DWConv are set as 7 for ATD-light and 5 for other versions of ATD.

A.1.3 Implementation Details

ATD. We follow previous works (Liang et al., 2021; Chen et al., 2023) and choose DF2K(DIV2K (Timofte et al., 2017) + Flickr2K (Lim et al., 2017)) as the training dataset for ATD. We split the training process for ATD into two stages. In the first stage, we randomly crop 64×64 LR patches and the corresponding HR image patches for training. The batch size is set as 64, while commonly used Data augmentation tricks including random rotation and horizontally flipping are adopted in our training stage. We adopt the AdamW (Loshchilov & Hutter, 2018) optimizer with $\beta_1 = 0.9, \beta_2 = 0.9$ to minimize L_1 pixel loss between HR estimation and ground-truth. For the case of zooming factor ×2, we train the model from scratch with an initial learning rate of 2×10^{-4} for 600k iterations. We then finetune the ×4 model based on ×2 model for 300k iteration. The learning rate gradually decay to 1×10^{-6} using cosine annealing scheduler (Loshchilov & Hutter, 2016). Then in the second stage, we utilize larger LR patches with size of 96×96 to further improve performance. The initial learning rate is reduced to 1×10^{-5} for stable finetuning process of 50k iteration.

ATD-light. To make fair comparisons with previous SOTA methods, we only employ DIV2K for training. Same as ATD, we train the ×2 model from scratch and the ×4 model is finetuned from ×2 one. We increase the batch size to 128 for ATD-light and thus we can apply a large initial learning rate of 1×10^{-3} for ×2 training process. The training procedure for ATD-light is identical to that of ATD, except we don't apply the large-patch finetune stage for ATD-light.

ATD-U. We choose ImageNet (Deng et al., 2009) as training data. To save training time, we first train ATD-U for 2000k iterations with a small window size of 8×8. Each batch consists of eight 128×128 noisy image patches. The initial learning rate is set as 2×10^{-4} and we halve it at [400k, 800k, 1200k, 1600k, 1800k, 1900k]. Then we expand the window size to 16×16 and apply a two-phase finetuning strategy. The patch size is first enlarged to 256×256 for 160k iterations and further up to 512×512 for another 120k iterations. In the final finetuning phase we change the training dataset to DFWB(DIV2K, Flickr2K, BSD500 (Arbelaez et al., 2011) and WED (Ma et al., 2017)). The initial learning rate for each finetuning phase is decreased to 1×10^{-5} for stability.

A.2 Additional Experimental Results

A.2.1 Experiments on Gaussian Color Image Denoising

Additional experiments were carried out with ATD-U model for Gaussian color image denoising, and the experimental setting keeps consistent with grayscale one. We compare ATD-U with several SOTA methods including DnCNN (Zhang et al., 2017a), RNAN (Zhang et al., 2019), RDN (Zhang et al., 2018b), IPT (Chen et al., 2020), DRUNet (Zhang et al., 2021), SwinIR (Liang et al., 2021), Restormer (Zamir et al., 2022), and ART (Zhang et al., 2023). Quantitative results on Kodak24 (Franzen, 1999) and Urban100 (Huang et al., 2015) are provided in Table 5. Experimental results show that our proposed ATD-U yields 0.43dB and 0.18dB performance gain over Restormer and ART under severe noise level of $\sigma = 50$, which demonstrate the superiority of ATD-U to these methods.

Table 5: Quantitative PSNR(dB) comparison with state-of-the-art methods on **color image denoising** task. Best and second best results are colored with red and blue.

Dataset	σ	DnCNN	RNAN	RDN	IPT	DRUNet	SwinIR	Restormer	ART	**ATD-U** (ours)
Kodak24	15	34.60	-	-	-	35.31	35.34	35.35	35.39	35.38
	25	32.14	-	-	-	32.89	32.89	32.93	32.95	32.99
	50	28.95	29.58	29.66	29.64	29.86	29.79	29.87	29.87	29.93
Urban100	15	32.98	-	-	-	34.81	35.13	35.13	35.29	35.36
	25	30.81	-	-	-	32.60	32.90	32.96	33.14	33.25
	50	27.59	29.08	29.38	29.71	29.61	29.82	30.02	30.27	30.45

A.3 More Visual Comparisons

We provide more visual comparisons on image super-resolution in Fig. 7, Fig. 8, Fig. 9, Fig. 10 and grayscale image denoising in Fig. 11. These visual comparisons illustrate the potential of ATD and ATD-U in restoring sharp edge and texture under severe degradation.

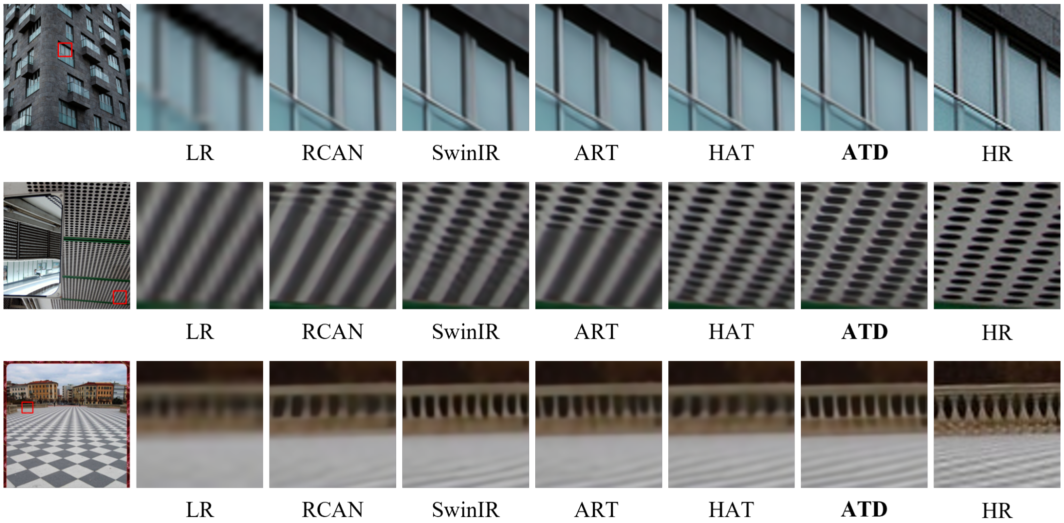
LR RCAN SwinIR ART HAT **ATD** HR
LR RCAN SwinIR ART HAT **ATD** HR
LR RCAN SwinIR ART HAT **ATD** HR

Figure 7: More visual comparisons of **classic image super-resolution** task on Urban100 (Huang et al., 2015) dataset. Test images from top to bottom are respectively "img_001", "img_004", "img_021".

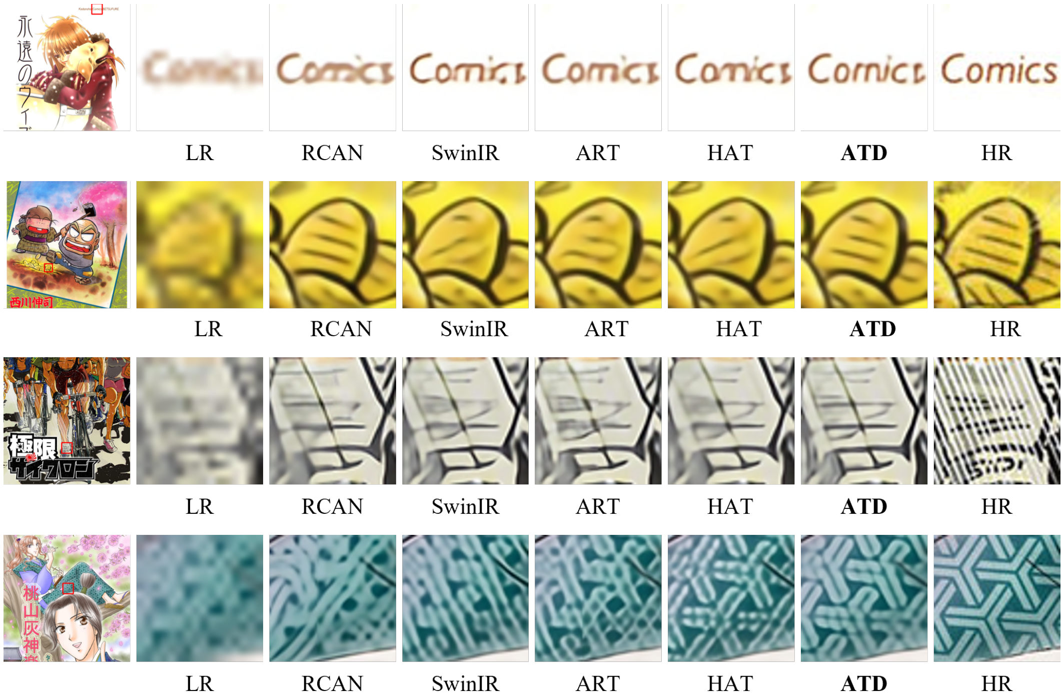
LR RCAN SwinIR ART HAT **ATD** HR
LR RCAN SwinIR ART HAT **ATD** HR
LR RCAN SwinIR ART HAT **ATD** HR
LR RCAN SwinIR ART HAT **ATD** HR

Figure 8: More visual comparisons of **classic image super-resolution** task on Manga109 (Matsui et al., 2016) dataset. Test images from top to bottom are respectively "EienNoWith", "JijiBabaFight", "KyokugenCyclone", "MomoyamaHaikagura".

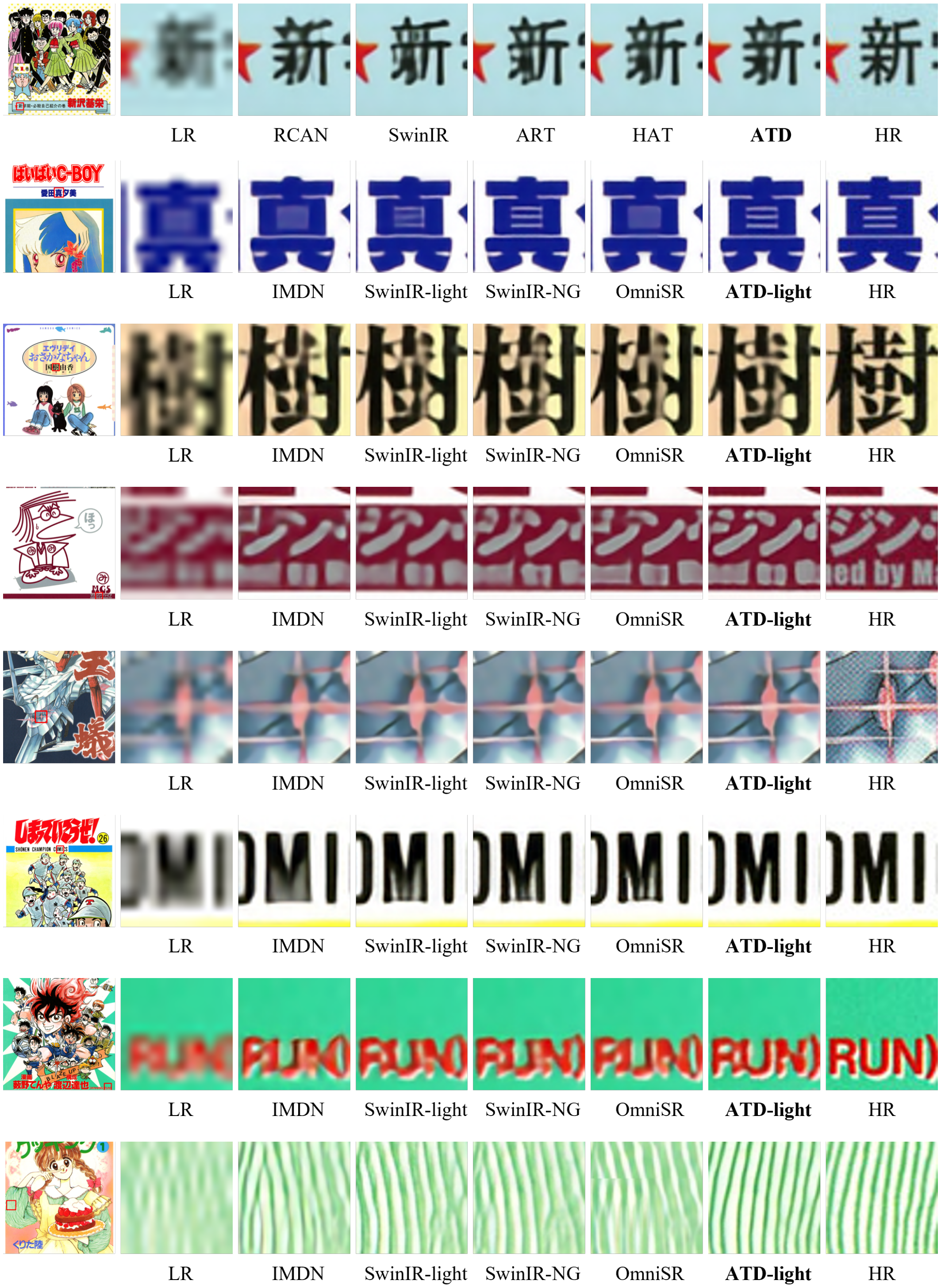

Figure 9: More visual comparisons of **classic image super-resolution** and **lightweight image super-resolution** task on Manga109 (Matsui et al., 2016) dataset. Test images from top to bottom are respectively "HighschoolKimengumi_vol01", "EverydayOsakanaChan", "Hamlet", "Joouari", "Shimattelkouze_vol26", "UltraEleven", "YumeiroCooking".

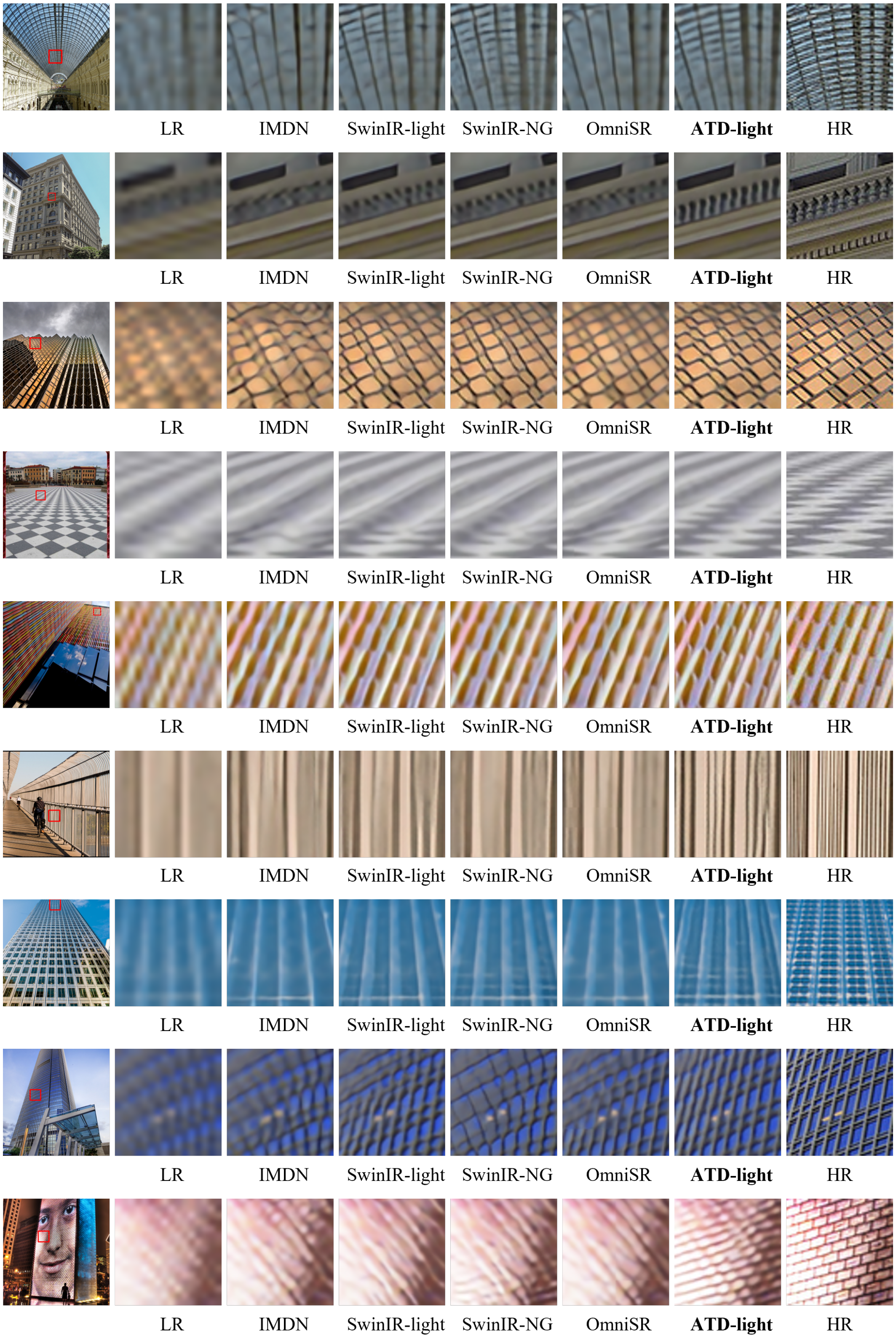

Figure 10: More visual comparisons of **lightweight image super-resolution** task on Urban100 (Huang et al., 2015) dataset. Test images from top to bottom are respectively "HighschoolKimengumi_vol01", "EverydayOsakanaChan", "Hamlet", "Joouari", "Shimattelkouze_vol26", "UltraEleven", "YumeiroCooking".

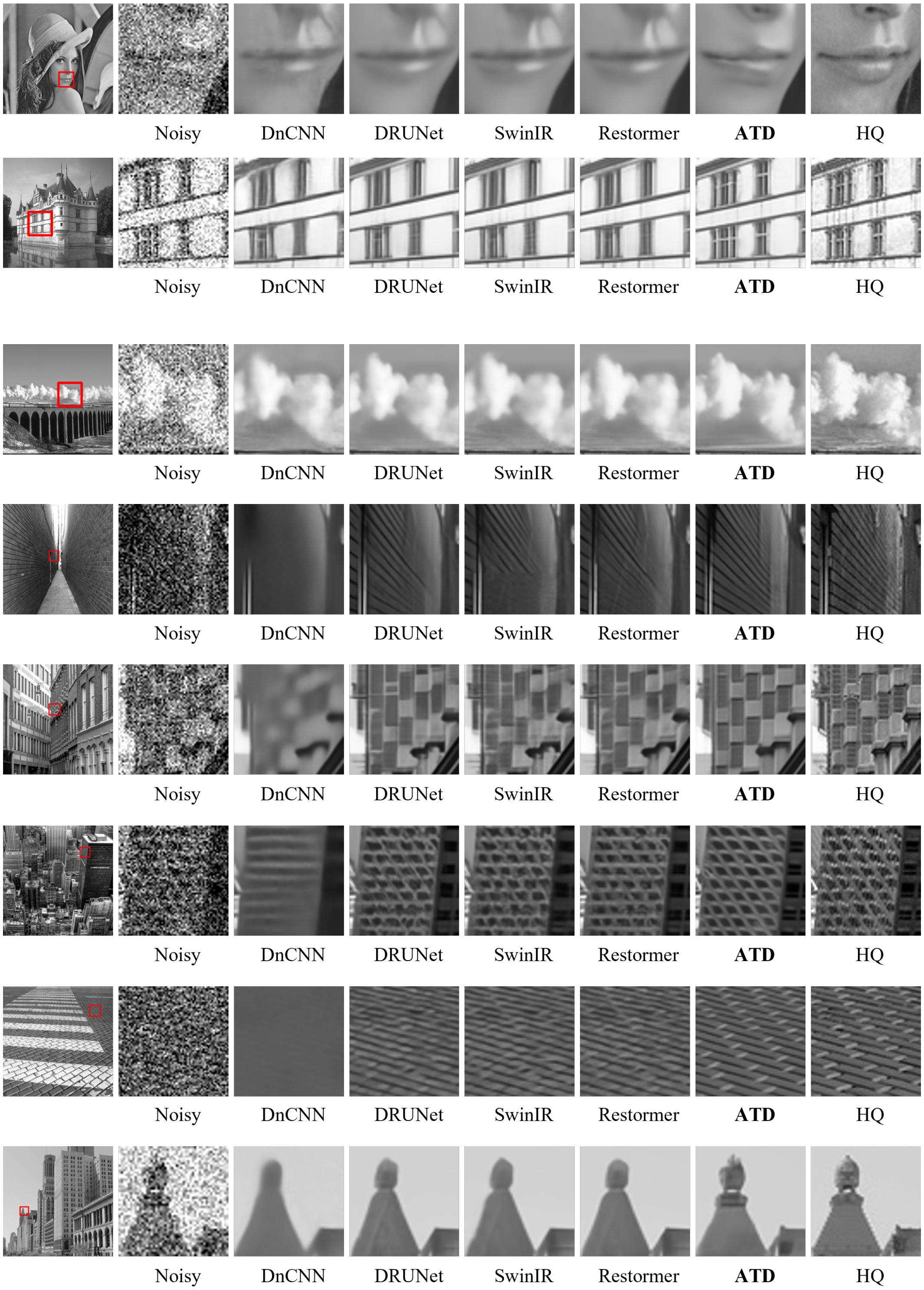

Figure 11: More visual comparisons of **grayscale image denoising** task. Test images from top to bottom are respectively "Lena" from Set12 (Zhang et al., 2017a), "test_003", "test_033" from BSD68 (Martin et al., 2001), and "img_038", "img_064", "img_073", "img_091", "img_097" from Urban100 (Huang et al., 2015) dataset.